Reduction Features of NO over a Potassium-Doped C12A7−O^- Catalyst

Aimei Gao,[†] Xifeng Zhu,[†] Huajing Wang,[†] Jing Tu,[†] Peiyan Lin,[†] Youshifumi Torimoto,[‡] Masayoshi Sadakata,[‡] and Quanxin Li*[,†]

Lab of Biomass Clean Energy, Department of Chemical Physics, University of Science and Technology of China, Hefei, Anhui 230026, People's Republic of China, and Department of Chemical System Engineering, School of Engineering, University of Tokyo, 7-3-1 Hongo, Bunkyo-ku, Tokyo 113-8656, Japan

Received: January 10, 2006; In Final Form: March 13, 2006

The NO reduction features over a noble-metal-free NO_x storage/reduction catalyst ($[Ca_{24}Al_{28}O_{64}]^{4+}\cdot 4O^-$/K, defined as C12A7−$O^-$/K), including the NO conversion, the N_2 selectivity, and sulfur tolerance, were investigated with hydrogen and C_3H_6 as the reducing agents in a fixed-bed continuous flow reactor. The NO conversion and the N_2 selectivity on the C12A7−O^-/K catalyst mainly depends on the sample temperature, the percentage of potassium, the reducing agents, and the composition of the mixture of gases. The C12A7−O^-/10%K catalyst possessed the highest selective reduction ability (to N_2) among the catalysts C12A7−O^-/*x*%K. Over 50% of NO can be reduced to N_2 with H_2 as the reduction agent at 550−700 °C. The C12A7−O^-/K catalyst also shows higher NO_x storage capacity (183.9 μmol/g at about 550 °C) as well as sulfur tolerance for both the NO_x storage and the reduction processes. The catalyst characteristics and the intermediate species formed in the NO storage and reduction processes were investigated by the X-ray diffraction, X-ray photoelectron spectroscopy, Fourier transform infrared spectroscopy, and time-of-flight mass spectrometry. The mechanism of NO_x reduction was addressed according to the above investigations.

1. Introduction

With continuously tightened legislation concerning the exhaust emissions of automobiles, it is of great importance to reduce emission of pollutants such as NO_x, CO, CO_2, SO_2, and hydrocarbons (HCs). However, traditional three-way catalysis (TWC) is not able to effectively reduce NO_x under excess oxygen (lean−burn) conditions. An alternative approach is the so-called NO_x storage/reduction (NSR) concept pioneered by Toyota.[1−3] In the NSR approach, NO_x is trapped in the catalyst during the relatively long lean period, and then NO_x stored as nitrites or nitrates is decomposed and subsequently reduced to nitrogen. There has been a lot of experimental and theoretical work by using various NSR catalysts, such as barium oxide, barium carbonate, Ba-based noble metal catalysts, Co/Ba catalysts, CuO/ZrS mixed with a solid base catalyst, and $H_3PW_{12}O_{40}\cdot 6H_2O$, etc.[3−16]

Selective catalytic reductions (SCRs) of nitric oxide by ammonia ($4NO + 4NH_3 + O_2 \rightarrow 4N_2 + 6H_2O$) and by hydrocarbons (NO + hydrocarbons $\rightarrow N_2 + CO_2 + H_2O$) have been extensively investigated over a variety of catalysts including noble metals,[17,18] ion-exchanged zeolites,[19−21] and metal oxides.[22] The well-reviewed papers for this technology have been published by Bosch and Janssen [23] and Amiridis et al.[24] But from a practical standpoint, the NH_3-based SCR technologies have problems such as NH_3 stoichiometric control and storage for practical transportation applications. A variety of hydrocarbons, ranging from methane,[25,26] ethene,[27,28] and propane/-ene[29−31] to larger molecules,[32] have been shown to selectively react with NO_x in the presence of excess oxygen. The hydrogen can be generated from the fuel, and the NO/H_2 reaction has been well investigated.[33−34] It was demonstrated that the hydrogen could be used to effectively reduce NO to N_2 under lean−burn conditions over platinum-based catalysts.[35] Mahzoul et al. have found that hydrogen was the most efficient reduction agent among H_2, CO, and C_3H_6 in terms of the conversion efficiency and reduction agent's usage efficiency when the conventional NO_x-trap catalyst was used.[4] Liu and Anderson also revealed that the order of the reduction efficiency was H_2 > CO > propene in terms of the conversion of the stored NO_x to N_2 over the Pt/Ba/Al_2O_3 NSR catalysts.[5]

It is well-known that the Ba-based catalysts are the most important NSR catalysts. But these catalysts have strong absorption for sulfur in real exhaust gases, which forms very stable sulfates on the catalysts. The sulfates inhibit the sustainable NO_x storage and reduction and finally lead to the deactivation of the NSR catalysts.[36−37] To improve the sulfur tolerance of the Ba-based catalysts, adding other elements such as Co, Ce, Fe, and noble metals, etc. has been reported.[12,38−39]

Active anion species O^- stored in the cages of the microporous material $12CaO\cdot 7Al_2O_3$ (C12A7−O^-) is a key intermediate in the anion chemistry,[40−45] and the material C12A7−O^- may be used as an active catalyst. For example, the C12A7−O^- catalyst can be used for direct synthesis of phenol from benzene with oxygen and water.[46] In our previous work, we have investigated Pt/$BaAl_2O_4$−Al_2O_3, $BaFeO_3$, and $BaZrO_3$ catalysts as a NO_x storage/reduction catalyst.[47−50] Here, we prepared a new NO_x storage/reduction catalyst C12A7−O^-/K, which possessed good NO_x storage/reduction ability with a high sulfur tolerance. In the present paper, we mainly focused on the NO reduction features and the reduction mechanism over the C12A7−O^-/K catalyst.

* Author to whom correspondence should be addressed. E-mail: liqx@ustc.edu.cn.
[†] University of Science and Technology of China.
[‡] University of Tokyo.

10.1021/jp060178t CCC: $33.50
Published on Web 05/27/2006

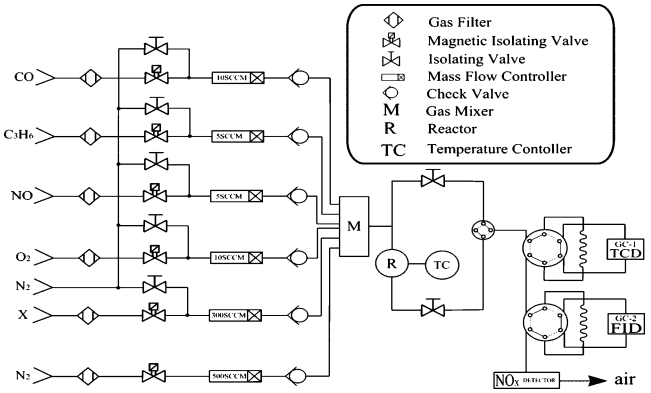

Figure 1. Schematic setup of the fixed-bed flow microreactor system for the NO_x storage/reduction experiments.

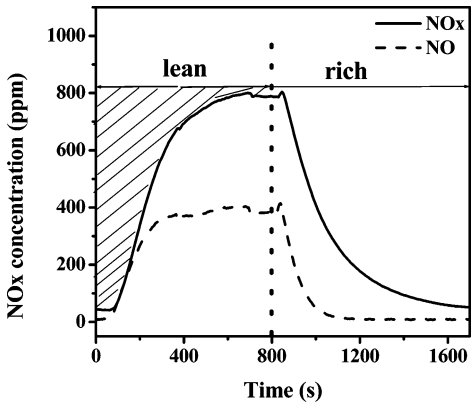

Figure 2. Example of the NO and NO_x ($NO + NO_2$) outlet traces for a single lean−rich cycle (i.e., the cycle from the NO storage ($NO/O_2/C_3H_6/Ar$ system) to the NO reduction ($NO/C_3H_6/Ar$ system). Lean conditions: NO_x 820 ppm, O_2 4.8%, C_3H_6 1200 ppm, Ar balance, lean time 800 s. Rich conditions: NO_x 820 ppm, C_3H_6 1200 ppm, Ar balance, rich time 900 s. Reaction conditions: catalyst volume 0.5 mL, total flow rate 210 mL/min, 500 °C.

2. Experimental Section

2.1. Catalyst Preparation. The C12A7−O⁻ sample was prepared by a solid-state reaction at 1350 °C for 16 h. A more detailed description of the process for preparation can be found elsewhere.[51−54] The C12A7−O⁻ pellet was also powdered and mechanically mixed with various contents of $KHCO_3$. Finally, these mixtures were calcined in air by a muffle furnace from room temperature to 900 °C and maintained at this temperature for 4 h. The initial $KHCO_3$ loading on C12A7−O⁻ was made using 20, 30, and 40% in weight percentage (wt %) of C12A7−O⁻. It was found that part of the potassium was lost from the catalyst in the heat treatment process. The final potassium contents on the potassium-based C12A7−O⁻ catalysts were 5.17, 9.69, and 12.80%, which was measured by inductively coupled plasma atomic emission spectroscopy (ICP-AES). This series of materials was defined as C12A7−O⁻/*x*%K (x = 5, 10, 13). Finally, all the sintered materials were crushed into granules (300−440 μm).

2.2. Flow-Reaction Experiments. The NO reduction experiments were performed in a conventional fixed-bed flow microreactor at atmospheric pressure (Figure 1). The reaction temperature was monitored by a thermocouple inserted in the catalyst bed. The reaction system was equipped with pressure indicators and mass flow controllers. A typical feeding composition was NO (4.33%), H_2 (2.6−13.8%), and O_2 (0−5%) in an Ar balance gas. All of the gases used were ultrahigh purity gases (99.999%). Product analysis was performed with on-line gas chromatography (GC) with a thermal conductivity detector (TCD). A quadropole mass spectrometer was also used to analyze the reaction products. The experiments were repeated three times. The difference for each replicate generally ranged from 0 to 20%. The results given are averages.

According to our investigation, it was found that the C12A7−O⁻/10%K catalyst gave the highest storage/reduction capacity among the catalysts C12A7−O⁻/*x*%K. Thus, much attention was paid to study the NO storage/reduction features of the C12A7−O⁻/10%/K catalyst. The NO reduction capacity was estimated by the percentage of NO conversion under reduction conditions

$$C_{NO} = ([NO]_{in} - [NO]_{out})/[NO]_{in} \quad (1)$$

where $[NO]_{in}$ and $[NO]_{out}$ are the inlet and outlet concentrations of NO, respectively. The reduction products were measured by on-line gas chromatography, from which the N_2 selectivity was obtained. The percentage of N_2 selectivity was calculated from

$$S_{N_2} = 2[N_2 \text{ in effluent}]/([NO]_{in} \times C_{NO}) \quad (2)$$

To study the initial NO_x storage/reduction activity, the NO and NO_x were measured under the lean−rich burn cycle conditions. $NO/NO_2/NO_x$ analysis was performed with an on-line 8840 chemiluminesence NO_x analyzer. Figure 2 shows a typical single lean−rich cycle (i.e, storage−release cycle). To clean the catalyst surface and recover the lean environment from the rich one in the present measurement system, the rich phase time is longer than the lean one. For each storage and release cycle, the catalyst was first exposed to the standard NO-containing adsorption mixtures under the lean−burn condition. After the saturation adsorption was reached, the O_2 flow was turned off, and the measurements were changed to the rich−burn condition. Because of the presence of the reducing agent under the lean condition, the definition of NO_x storage in Figure 2 actually means the coexistence of storage and reduction processes. The total amount of NO_x stored during the lean period can be obtained by integrating the shaded section in Figure 2. The NO_x storage capacity (NSC) was calculated from the total stored amount in micromoles, divided by the weight of the catalyst.

2.3. Catalyst Characterization. *2.3.1. Inductively Coupled Plasma Atomic Emission Spectroscopy.* The total doped metal contents in the prepared C12A7−O⁻/*x*%K catalysts were estimated by ICP-AES using an Atomscan Advantage ICP-AES system (Thermo Jarrell Ash Co.).

2.3.2. X-ray Diffraction. The catalysts were studied by X-ray diffraction (XRD) before and after the NSR experiments. The samples were generally crushed into a powder with an average diameter of 20−30 μm. X-ray diffraction patterns of the catalysts were recorded on an X'pert Pro Philips diffractrometer, using a Cu Kα radiation (λ = 0.15418 nm). The measurement conditions were in the 2θ range 10−70°, step counting time 5 s, and step size 0.017° at 25 °C.

2.3.3. X-ray Photoelectron Spectroscopy. The X-ray photoelectron spectroscopy (XPS) measurements were performed on a VG ESCALAB MKII instrument, using Mg Kα primary radiation (15 kBV, 10 mA). The binding energy scale was corrected by using C(1s) at 284.6 eV as a standard.

2.3.4. Fourier Transform Infrared Spectroscopy. Fourier transform infrared (FTIR) spectra were measured at 298 K by a Bruker EQUINOX55 FTIR spectrometer with the KBr pellet method. The samples for FTIR measurements were mixed at a weight ratio of sample/KBr = 100:3, then ground and pressed by a pressure of 400 atm to a pellet with a diameter of 1.0 cm

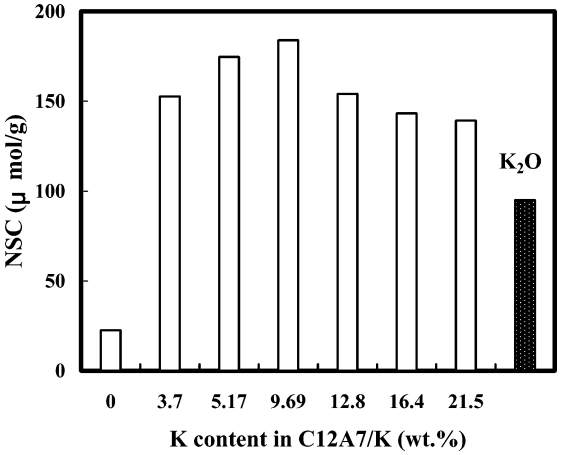

Figure 3. Effect of potassium content on NO_x storage capacity for C12A7−O^-/*x*%K at 550 °C. Reaction conditions: NO 750 ppm, O_2 4.8%, N_2 balance, catalyst volume 0.5 mL, total flow rate 210 mL/min.

and a thickness of 1.0 mm. The infrared absorption spectra were recorded and analyzed.

2.3.5. Time-of-Flight Mass Spectrometry. The intermediates formed from the surface reactions of the catalysts were mass analyzed by a time-of-flight (TOF) mass spectrometer at a background vacuum of about 1×10^{-4} Pa, and the experimental apparatus has been described in detail in refs 55 and 56. The C12A7−O^- sample with a diameter of 15 mm and a thickness of 1 mm was fixed in the middle of the sample chamber, and the reactants (e.g., NO or NO/O_2) were fed onto the front-side surface of C12A7−O^- by a nozzle with a chamber pressure of about 5×10^{-3} Pa.

3. Results and Discussion

3.1. Features of NO Storage over C12A7−O^-/K Catalysts. Figure 3 shows the effect of the potassium content on the NO_x storage capability of the C12A7−O^-/*x*%K catalysts at 550 °C under a given flowing gas mixture (NO_x 750 ppm, O_2 4.8%, and N_2 balance gas). It was found that the addition of potassium to the catalysts significantly increased the NO_x storage capability and reached a maximum value about 183.9 μmol/g at a potassium content about 10% in the sample. Further increasing potassium content (over 10%) resulted in the decrease of the NO_x storage capability. However, the pure C12A7−O^- and K_2O samples were also tested. Even though the pure K_2O and C12A7−O^- show somewhat of a NO_x storage capability, the apparent NSC of C12A7−O^-/*x*%K is not a simple sum between the NSC value of K_2O and that of C12A7−O^-. The above results may suggest that the addition of potassium plays a synergetic effect in the NO_x storage over the C12A7−O^-/*x*%K catalysts.

The reaction temperature also affects the NO_x storage capacity. In the temperature range of 200−550 °C, the NSC of C12A7−O^-/10%K increases with increasing temperature and reaches a maximum value of 183.9 μmol/g at about 550 °C. At temperatures over 550 °C, NSC decreases with rising temperature. An optimum temperature window for NO_x storage with C12A7−O^-/10%K catalyst ranges from 400 to 650 °C. Moreover, the NSC value and the sulfur tolerance of the C12A7−O^-/10%K catalyst was compared with our other NSR catalysts (Table 1). The NSC of C12A7−O^-/10%K catalyst is close to the levels of $Rh/BaZrO_3/Al_2O_3$ and $BaZrO_3$ but lower than that of the $Pt/BaAl_2O_4/Al_2O_3$ catalyst. However, the C12A7−O^-/K catalyst has a higher sulfur tolerance in comparison with $Pt/BaAl_2O_4/Al_2O_3$.

TABLE 1: NO_x Storage Capacities and the Sulfur Tolerances of Different Types NO_x Storage/Reduction Catalysts[a]

		NSC[b] (μmol/g)	
samples	T(°C)	without SO_2	with 100 ppm SO_2
$BaFeO_3$	400	114.7	93.5
$Pt/BaAl_2O_4-Al_2O_3$	400	340.1	50.9
$BaZrO_3$	400	175.4	175.6
$Rh/BaZrO_3/Al_2O_3$	400	202.2	241.6
C12A7−O^-/10%K	550	183.9	203.7

[a] NO_x stored condition: NO_x 750 ppm, O_2 4.8%, N_2 balance gas, flow rate 210 mL/min, catalyst volume 0.5 mL. [b] The NSC values given are the averages derived from the lean periods of the second through fourth cycles over different catalysts.

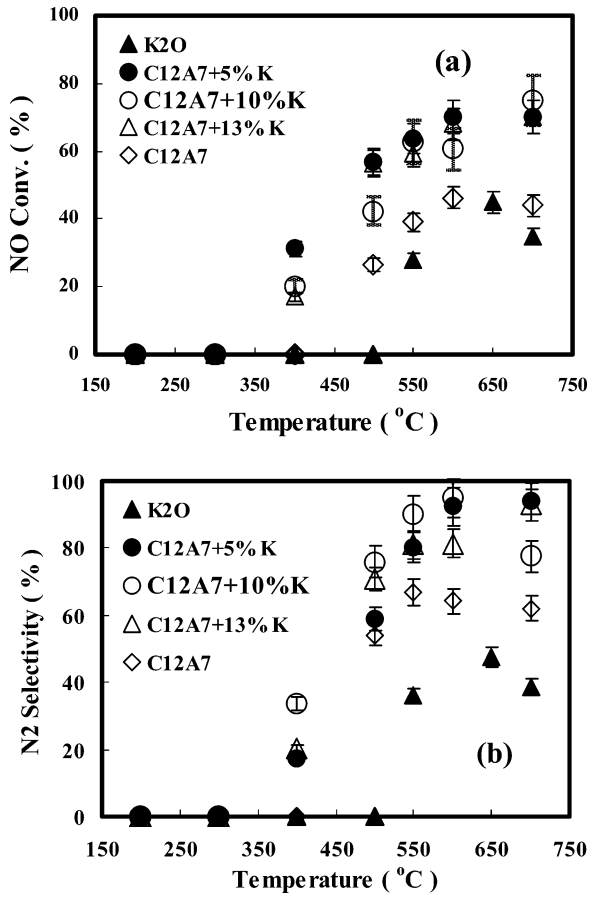

Figure 4. NO conversion and N_2 selectivity measured as a function of the temperature at different potassium concentrations over C12A7−O^-/*x*%K catalyst. Reaction conditions: NO 4.33%, H_2 8.15%, Ar balance, catalyst volume 1.0 mL, total flow rate 30 mL/min.

3.2. Features of the NO reduction over C12A7−O^-/K Catalysts. *3.2.1. Effects of the Percentage of Potassium on NO Reduction.* Figures 4a and 4b show the effect of the potassium content on the NO conversion and the N_2 selectivity of the C12A7−O^-/*x*%K (*x* stands for the weight percent of potassium in the samples) catalysts under a given flowing gas mixture (NO 4.33%, H_2 8.15%, Ar balance, catalyst 1.0 mL, total flow rate 30 mL/min). It was found that the addition of potassium to the catalysts significantly enhanced the NO reduction capability, and the optimum potassium concentration for converting NO to N_2 was about 10%. Even though C12A7−O^- and K_2O show some of the NO reduction activation, their NO conversion activities are much lower than that of C12A7−O^-/*x*%K. The addition of potassium to C12A7−O^- may play a synergetic effect in the NO reduction over the C12A7−O^-/K catalysts. The promoting effects of adding sodium to Pt/Al_2O_3 catalyst

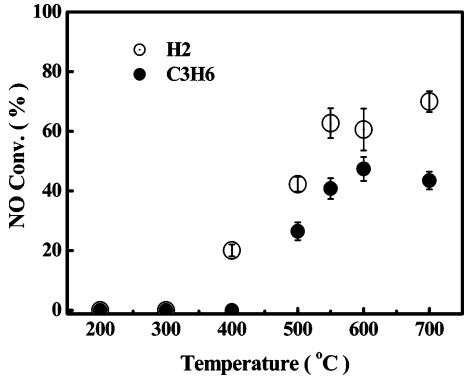

Figure 5. Temperature effects on the conversion of NO for C12A7−O⁻/10%K catalyst by different reducing agents. Reaction conditions: NO 4.33%, H_2 8.15% or C_3H_6 8.3%, Ar balance, catalyst volume 1.0 mL, total flow rate 30 mL/min.

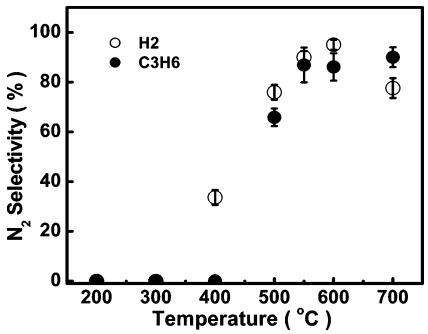

Figure 6. Temperature effects on the selectivity of N_2 for C12A7−O⁻/10%K using H_2 and C_3H_6 as a reducing agents. Reaction conditions: NO 4.33%, H_2 8.15% or C_3H_6 8.3%, Ar balance, catalyst volume 1.0 mL, total flow rate 30 mL/min.

on the NO reduction and the N_2 selectivity were also found by Burch and Coleman.[57] This promoting effect could be attributed to the increase of the Lewis base and enhance the reactions between H_2 and NO_2. On the basis of the overall evaluation for the NO_x storage capacity, NO reduction ability, and the N_2 selectivity, the optimum percentage of potassium is about $x =$ 10 wt % in C12A7−O⁻/K.

3.2.2. Effect of Temperature on NO Reduction by the Different Reducing Agents. Figure 5 shows the effect of temperature on the NO conversion over the C12A7−O⁻/10%K catalyst by H_2 and C_3H_6 as the reducing agent, respectively, under typical reduction conditions (NO 4.33%, H_2 8.15% or C_3H_6 8.3%, Ar balance, catalyst volume 1.0 mL, total flow rate 30 mL/min). When H_2 is used as the reducer, the NO conversion increases with increasing temperature in the temperature range of 200−700 °C and reaches about 70% at 700 °C. At temperatures over 550 °C, the NO conversion increased smoothly with rising temperature. An optimum operating temperature window for the NO conversion with C12A7−O⁻/10%K catalyst ranges from 500 to 700 °C. In comparison with the H_2 reducing agent, the most significant difference using H_2 and C_3H_6 as the reducing agents is that the ignition temperature of the NO reduction by H_2 (about 550°C) is lower than that by C_3H_6 (about 600 °C).

It is noted that in the reduction of NO the selectivity of N_2 rather than N_2O is important because N_2O itself is a pollutant. Figure 6 shows the dependence of the N_2 selectivity on the sample temperature over C12A7−O⁻/10%K. For H_2, the N_2 selectivity increases with increasing temperature in the range of 200−600 °C and reaches a maximum value of about 95% at about 600 °C. Over 600 °C, the N_2 selectivity appears to slightly decrease. Over 50% of NO can be reduced to N_2 by using H_2 as a reduction agent at 550−700 °C, which is close to the performance of the Pt/Al_2O_3 catalyst.[57] When C_3H_6 was used as the reducing agent, the ignition temperature of N_2 selectivity becomes higher than that of H_2. The temperature behavior of the N_2 selectivity should reflect the channel competition from NO converting to N_2 and N_2O.

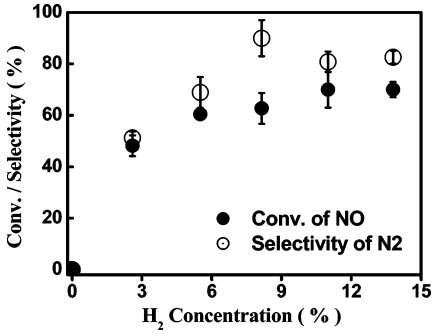

Figure 7. H_2 concentration effects on the conversion of NO and the selectivity of N_2 at 550 °C for C12A7−O⁻/10%K. Reaction conditions: NO 4.33%, H_2 0−13.8%, Ar balance, catalyst volume 1.0 mL, total flow rate 30 mL/min.

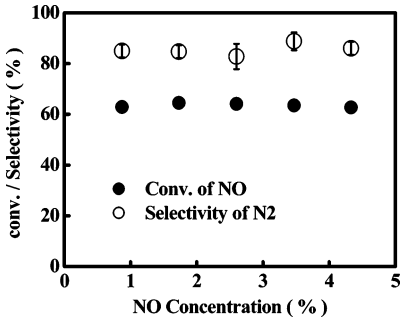

Figure 8. NO concentration effects on the conversion of NO and the selectivity of N_2 at 550 °C for C12A7−O⁻/10%K under the fixed H_2/NO ratio of 1.9. Reaction conditions: NO 0.87−4.33%, H_2 1.63−8.13%, Ar balance, catalyst volume 1.0 mL, total flow rate 30 mL/min.

3.2.3. Effects of the H_2, NO, and O_2 Concentrations on NO Reduction. Figure 7 shows the NO conversion measured as a function of the H_2 concentration over C12A7−O⁻/10%K catalyst at a temperature of 550 °C. When H_2 is absent in the feeding gas, the NO conversion on C12A7−O⁻/10%K is close to zero within our detecting sensitivity. The NO conversion obviously increased with the increasing H_2 content in the reduction mixtures. On the other hand, the N_2 selectivity also depends on the H_2 concentration, as shown in Figure 7, giving a maximum value about 90% at the H_2/NO ratio of 1.9. The N_2 selectivity slightly decreased at higher H_2 concentrations.

Figure 8 shows NO concentration effects on the conversion of NO and the selectivity of N_2 at 550 °C for C12A7−O⁻/10%K under the fixed H_2/NO ratio of 1.9. No significant changes of the NO conversion and the N_2 selectivity were found in the NO concentration range of 0.87−4.33%. Figure 9 shows the NO conversion and the N_2 selectivity measured as a function of the temperature at three different O_2 concentrations (0, 1.7, and 5%) over C12A7−O⁻/10%K catalyst. The promoting effect by O_2 on the NO conversion was observed. However, both the reduction capability and the N_2 selectivity decreased with increasing the O_2 content in the reduction mixtures (Figure 9b). The NO reduction rate and the N_2 selectivity depend on the ratio of oxygen to the reducing agent and the kinetic equilibrium in the reaction system.

3.3. Sulfur Tolerance of C12A7−O⁻/K. The behavior of resistance to sulfur poisoning is very important for a NO_x

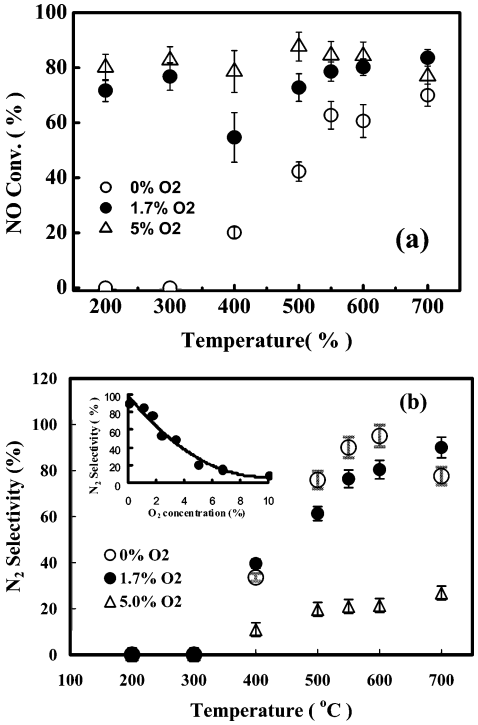

Figure 9. NO conversion and N_2 selectivity measured as a function of the temperature at three different O_2 concentrations (0, 1.7, and 5%) over C12A7−O^-/10%K catalyst. The inset shows the N_2 selectivity vs O_2 concentration in the range of 0−10%. Reaction conditions: NO 4.33%, H_2 8.15%, Ar balance, catalyst volume 1.0 mL, total flow rate 30 mL/min.

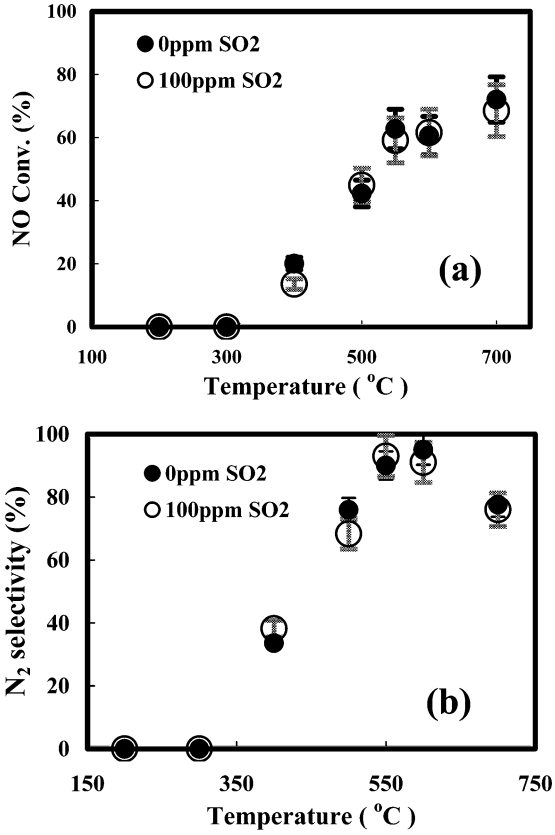

Figure 10. NO conversion and N_2 selectivity measured as a function of temperature under two reduction conditions, i.e., without SO_2 and with 100 ppm SO_2. Other conditions: NO 4.33%, H_2 8.15%, Ar balance, catalyst volume 1.0 mL, total flow rate 30 mL/min.

storage/reduction catalyst since sulfurets generally exist in the exhaust NO_x mixtures. SO_2 is formed from through the oxidation of sulfur compounds in the fuel and may result in a decrease of the NO_x storage/reduction capability. Figure 10 shows the NO conversion and the N_2 selectivity measured as a function of the temperature under two different reduction conditions (with and without SO_2). No significant influences on the NO reduction capability were observed with 100 ppm SO_2. Also, no sulfates were found on the reacted catalysts' surfaces based on the investigations by XRD, XPS, and FTIR (see section 3.4). The above result shows that the C12A7−O^-/K is expected to be a good sulfur tolerance catalyst.

3.4. Characterization. *3.4.1. X-ray Diffraction.* X-ray diffraction measurements were employed to investigate the crystal structure characteristics of C12A7−O^-/K catalysts and their changes resulting from the NO storage/reduction process with and without SO_2. Five different samples were measured by X-ray diffraction, i.e., (1) the initial C12A7−O^- sample, (2) the initial C12A7−O^-/10%K sample, (3) the NO_x stored C12A7−O^-/10%K sample, (4) the NO_x stored C12A7−O^-/10%K sample followed by H_2 reduction treatment, and (5) the NO_x stored C12A7−O^-/10%K sample (containing 100 ppm SO_2). Figure 11a shows the XRD spectrum for the C12A7−O^- sample, in which the peaks marked by asterisks have been assigned to the lattice framework of C12A7 by comparing the peak positions and intensities of the XRD pattern with the data in the Joint Committee on Powder Diffraction Standards (JCPDS) cards. In Figure 11b, the peak intensities of the XRD spectrum for the K-doped C12A7−O^- sample (i.e., C12A7−O^-/10%K) decrease as compared with those of the fresh C12A7−O^-, and some weak peaks (for example, peaks at 2θ = 47.8° and 59.3°) disappear for C12A7−O^-/10%K which appear for C12A7−O^-. They are attributed to the concentration decrease of C12A7−O^- in C12A7−O^-/10%K. But the C12A7−O^- sample after doping potassium does not destroy the positively charged lattice framework structure of C12A7−O^-. Even though the presence of K_2O in the C12A7−O^-/10%K sample has been proven by the XPS and FTIR measurements, no crystal structure of K_2O was observed by the XRD spectrum.

Figure 11c shows the XRD spectrum for NO_x stored C12A7−O^-/10%K after the NO storage treatment for 1.5 h under the typical oxidation conditions: NO_x 750 ppm, O_2 4.8%, N_2 balance gas, 550 °C. Beside the peaks corresponding to the C12A7−O^- structure, several weak and reproducible peaks at 2θ = 23.9°, 29.4°, and 33.8° appeared for the NO_x stored C12A7−O^-/10%K sample (see Figure 11c and the enlarged part shown in Figure 11g). By comparison of the crystal phase positions of KNO_3, these new peaks were attributed to KNO_3 formed by the reactions of NO_x with K_2O under the NO storage procedure. After further treatment of the NO_x stored C12A7−O^-/10%K sample by H_2 reduction for 0.6 h (i.e., the NO_x stored and reduced C12A7−O^-/10%K sample), the KNO_3 peaks fully disappeared (Figure 11d and the enlarged part shown in Figure 11h). Figure 11e shows the XRD spectrum for C12A7−O^-/10%K after the NO storage treatment for 1.5 h under the SO_2-containing conditions: SO_2 100 ppm, NO_x 750 ppm, O_2 4.8%, N_2 balance gas, 550 °C. The KNO_3 peaks were also observed in Figure 11e. According to the above XRD results, it was found that the intermediate of KNO_3 was formed during the NO_x storage process, which was reduced by H_2. No sulfate species were observed for the NO_x storage/reduction processes when 100 ppm SO_2 was contained in the mixtures.

3.4.2. Fourier Transform Infrared Spectroscopy. To investigate the intermediate species on the C12A7−O^-/K surface formed in the NO_x storage/reduction processes, the FTIR spectra were recorded for the following different samples: (1) the fresh

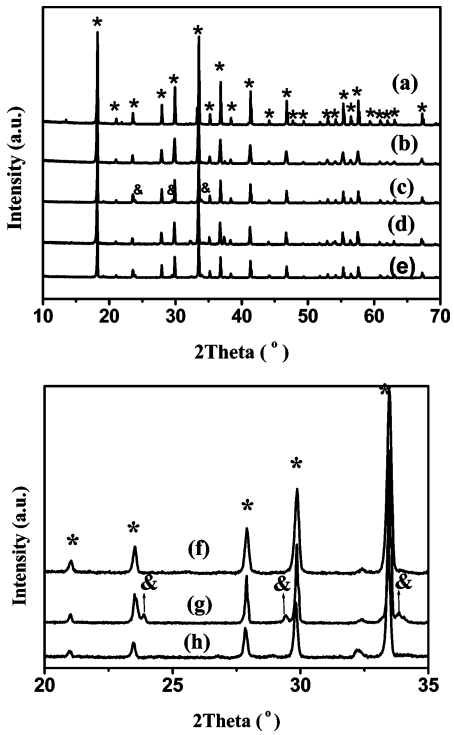

Figure 11. X-ray diffraction pattern spectra for (a) the C12A7−O⁻ sample, (b) the initial C12A7−O⁻/10%K sample, (c) the NO_x stored C12A7−O⁻/10%K sample, (d) the NO_x stored and reduced C12A7−O⁻/10%K sample, and (e) the NO_x stored C12A7−O⁻/10%K sample (containing 100 ppm SO_2). Spectra f, g, and h are enlargements of spectra b, c, and d, respectively. NO_x stored condition: NO_x 750 ppm, O_2 4.8%, N_2 balance gas, 550 °C. NO reduced condition: pure H_2, 550 °C. SO_2-containing storage condition: SO_2 100 ppm, NO_x 750 ppm, O_2 4.8%, N_2 balance gas, 550 °C. The peaks marked with asterisks have been assigned to the structure of C12A7, and those with ampersands have been assigned to the structure of KNO_3.

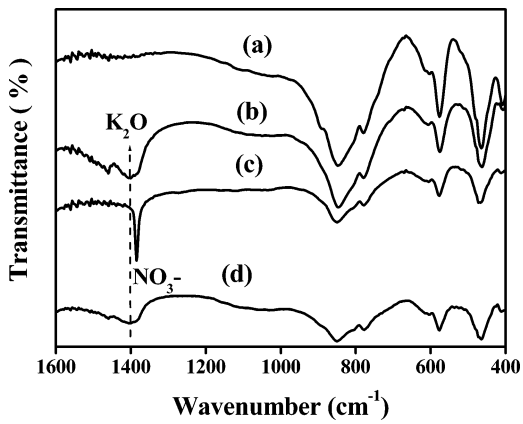

Figure 12. Fourier transform infrared spectra for (a) the initial C12A7−O⁻ sample, (b) the initial C12A7−O⁻/10%K sample, (c) the NO_x stored C12A7−O⁻/10%K sample (stored condition: NO_x 750 ppm, O_2 4.8%, N_2 balance gas, 550 °C for 1.5 h), and (d) the NO_x stored and then reduced C12A7−O⁻/10%K sample (stored condition: NO_x 750 ppm, O_2 4.8%, N_2 balance gas, 550 °C for 1.5 h; reduced condition: pure H_2, 550 °C for 0.6 h).

C12A7−O⁻, (2) the fresh C12A7−O⁻/10%K, (3) the NO_x stored C12A7−O⁻/10%K, (4) the NO_x stored C12A7−O⁻/10%K followed by H_2 reduction treatment. Figure 12a displays the FTIR spectra of the C12A7−O⁻ sample. The absorption in the 450−850 cm^{-1} region is attributed to the C12A7 characteristic absorption structures, corresponding to the Al−O stretching and bending modes in AlO_4 tetrahedra.[58] Figure 12b shows the FTIR spectrum of the potassium-doped C12A7−O⁻/10%K sample. A new broad peak around 1400.9 cm^{-1} was observed and attributed to K_2O. For the NO_x stored C12A7−O⁻/10%K catalyst (Figure 12c), there is a sharp peak near 1384.2 cm^{-1}, which is assigned to NO_3^- based on previous work.[59−60] It was also found that the sharp peak at 1384.2 cm^{-1} (NO_3^- peak) disappeared as we reduced the NO_x stored C12A7−O⁻/10%K catalyst by H_2 for 0.6 h (Figure 12d), which indicated that the NO_3^- species formed in the NO_x storage step reacted with H_2. Also, no sulfate peaks appeared in the NO storage/reduction process, as the NO mixture contains 100 ppm SO_2 (not shown here).

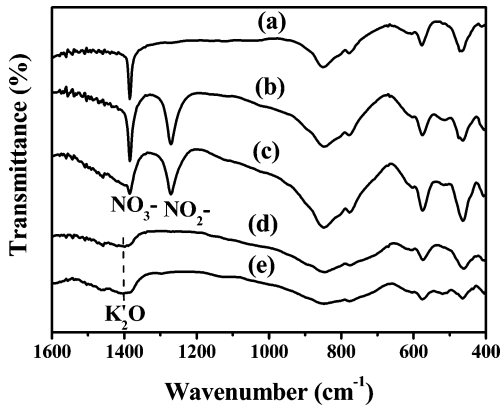

Figure 13. Fourier transform infrared spectra showing the C12A7−O⁻/10%K sample run under the following treatments: (a) NO_x storage for 1.5 h (NO_x 750 ppm, O_2 4.8%, N_2 balance gas, 550 °C), (b) the oxygen-containing reduction (NO 4.33%, H_2 8.15%, O_2 1.7%, Ar balance, flow rate 30 mL/min, temperature rising from 200 to 700 °C at 2 °C/min), (c) storage for 3 h (NO_x 4.33%, O_2 4.8%, Ar balance, 550 °C) followed by reduction (5% H_2 in Ar, flow rate 10 mL/min, rising from 200 to 700 °C at 10 °C/min), (d) storage for 3 h (NO_x 4.33%, O_2 4.8%, Ar balance, 550 °C) followed by reduction for 0.6 h (pure H_2, flow rate 25 mL/min, 550 °C), (e) NO reduction without O_2 (NO 4.33%, H_2 8.15%, Ar balance, flow rate 30 mL/min, temperature rising from 200 to 700 °C at 2 °C/min).

Figure 13 shows the FTIR spectra of the C12A7−O⁻/10%K sample run under the following treatments: (1) NO storage with 4.8% O_2, (2) NO storage/reduction by the mixture gas containing H_2 and O_2, (3) NO storage at 550 °C for 3 h and followed by the 5% H_2 reduction, (4) NO storage at 550 °C for 3 h followed by the pure H_2 reduction, **(**5**)** the NO reduction by H_2 without O_2. It was found that the NO_3^- species formed in the NO_x storage step was partly reduced into the NO_2^- species by the reaction of the NO_3^- species with H_2 (Figures 13b and 13c). Upon the reduction by pure H_2, the formed NO_3^- completely disappeared (Figure 13d). No nitrate or nitrite peaks appeared when NO was reduced by H_2 in the absence of O_2 (Figure 13e).

On the basis of the FTIR measurements, it can be concluded that (1) K_2O exists on the C12A7−O⁻/10%K surface, (2) NO_3^- is an important intermediate on the surface of the NO_x stored C12A7−O⁻/10%K catalyst, and (3) NO_3^- is able to be reduced by H_2 and no sulfate species on the catalyst's surface were found for the NO_x storage/reduction processes containing 100 ppm SO_2.

3.4.3. X-ray Photoelectron Spectroscopy. Four different samples (C12A7−O⁻, C12A7−O⁻/10%K, NO_x stored C12A7−O⁻/10%K, NO_x stored and reduced C12A7−O⁻/10%K) were investigated. Figure 14a shows the XPS spectrum for the C12A7−O⁻ sample, in which the peaks at 73.5, 347.0, and 531.3 eV have been assigned to Al(2p), Ca($2p_{3/2}$), O(1s) by comparing the peak positions with the data in the National Institute of Standards and Technology Databases. For the

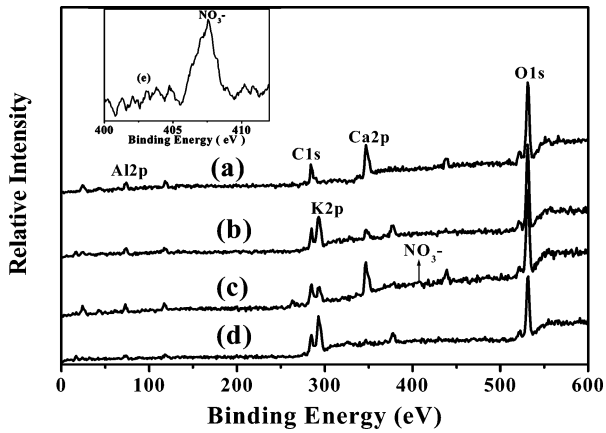

Figure 14. X-ray photoelectron spectra of (a) the initial C12A7−O^- sample, (b) the initial C12A7−O^-/10%K sample, (c) the NO_x stored C12A7−O^-/10%K sample, and (d) the NO_x stored C12A7−O^-/10%K sample followed by H_2 reduction. NO_x stored condition: NO_x 750 ppm, O_2 4.8%, N_2 balance gas, 550 °C for 1.5 h. The H_2-reduced condition: pure H_2, 550 °C for 0.6 h.

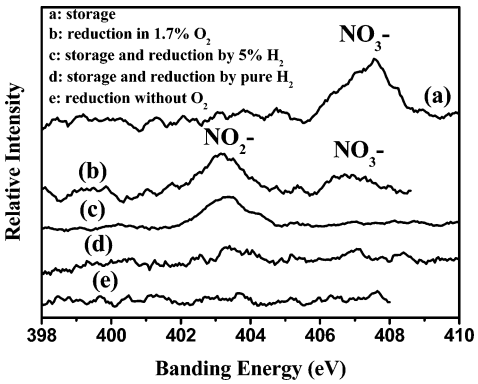

Figure 15. X-ray photoelectron N(1s) spectra of for C12A7−O^-/10%K in different conditions: (a) NO_x storage for 1.5 h (NO_x 750 ppm, O_2 4.8%, N_2 balance gas, 550 °C), (b) the oxygen-containing reduction (NO 4.33%, H_2 8.15%, O_2 1.7%, Ar balance, flow rate 30 mL/min, temperature rising from 200 to 700 °C at 2 °C/min), (c) storage for 3 h (NO_x 4.33%, O_2 4.8%, Ar balance, 550 °C) followed by 5% H_2 reduction (5% H_2 in Ar, flow rate 10 mL/min, temperature rising from 200 to 700 °C at 10 °C/min), (d) storage for 3 h (NO_x 4.33%, O_2 4.8%, Ar balance, 550 °C) followed by the pure H_2 reduction for 0.6 h (pure H_2, flow rate 25 mL/min, 550 °C), (e) NO reduction without O_2 (NO 4.33%, H_2 8.15%, Ar balance, flow rate 30 mL/min, temperature rising from 200 to 700 °C at 2 °C/min).

C12A7−O^-/10%K sample, the K($2p_{3/2}$) peak at 292.5 eV was observed (Figure 14b). As shown in Figure 14c, there was a new peak ranging from 405.5 to 409.3 eV for NO-stored C12A7−O^-/10%K that was attributed to NO_3^-.[61] It was also found that the peak for NO_3^- disappeared when the NO_x stored sample was further reduced by H_2 (Figure 14d). The above XPS results further confirmed that NO_x was converted to NO_3^- in the NO_x storage step and reduced in the H_2 reduction process. In addition, when 100 ppm SO_2 was added to the NO_x mixtures, we did not find any signal corresponding to SO_4^{2-}.

Figure 15 shows the XPS N(1s) spectra of for C12A7−O^-/10%K in different conditions: **(1)** NO storage, **(2)** NO storage/reduction by the mixture gas containing H_2 and O_2, **(3)** NO storage at 550 °C for 3 h followed by the 5% H_2 reduction, (4) NO storage at 550 °C for 3 h followed by the pure H_2 reduction, (5) NO reduction by H_2 without O_2. The XPS results also show that the NO_3^- species formed in the NO_x storage step can be partly reduced into the NO_2^- species by the reaction of the NO_3^- species with H_2 (Figure 15b).

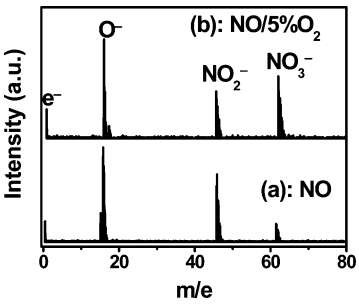

Figure 16. Time-of-flight mass spectra for the reaction systems (a) NO/C12A7−O^- and (b) NO/5% O_2/C12A7−O^-. Reaction conditions: 5×10^{-3} Pa, 630 °C.

TABLE 2: Binding Energies of O(1s) and K($2p_{3/2}$) for Different Samples

samples	O(1s) (eV)	K($2p_{3/2}$) (eV)
C12A7−O^-	531.3	
C12A7−O^-/10%K	531.1	292.5
NO_x stored C12A7−O^-/10%K	531.1	293.0

The binding energies of O(1s) and K($2p_{3/2}$) for different samples are given in Table 2. In comparison with the initial C12A7−O^-, the peak position of O(1s) for C12A7−O^-/10%K is slightly shifted from 531.3 eV to the low binding energy of 531.1 eV, which may be caused by the synergetic interaction between C12A7−O^- and the doped K_2O. And the peak position of K($2p_{3/2}$) for the NO_x stored C12A7−O^-/10%K is shifted from 292.5 to 293.0 eV in comparison with that of the initial C12A7−O^-/10%K.

3.4.4. Anionic Intermediates Desorbed from the C12A7−O^- Surface Detected by Time-of-Flight Mass Spectrometry. To investigate the intermediates of the NO reaction on the catalyst surface, TOF measurements have been performed under low-pressure conditions ($\sim 5 \times 10^{-3}$ Pa). It has been confirmed that the anions of O^- were able to desorb from the surface of C12A7−O^-.[55−56] When NO was fed onto the C12A7−O^- surface, two new peaks appeared at the mass numbers of 46 and 62, corresponding to NO_2^- and NO_3^-, respectively (Figure 16a). And the peak intensity of NO_2^- is larger than that of NO_3^-. As NO/5%O_2 was injected onto the C12A7−O^- surface, a similar spectrum was also observed (Figure 16b). However, the peak intensity of NO_3^- obviously increased. The above result shows that intermediates of NO_2^- and NO_3^- were formed by the reactions of O^-(surface)/O_2^-(surface) with NO/NO_2 on the C12A7−O^- surface (i.e., NO(s) + O^-(s) → NO_2^-(s), NO(s) + O_2^-(s) → NO_3^-(s), and NO_2(s) + O^-(s) → NO_3^-(s), where s represents the surface). Similar reactions were also found on the K-doped C12A7−O^- surface.

3.5. Mechanism of NO_x Storage/Reduction on C12A7−O^-/K. This study indicates that the C12A7−O^-/K catalyst, containing two compositions of C12A7−O^- and K_2O, possesses good NO_x storage and reduction abilities. The K_2O component plays a key role in the NO_x storage process under oxidizing conditions (i.e., feeding NO/O_2/Ar into the C12A7−O^-/K catalyst). In fact, it was found that the NSC over pure K_2O was significantly higher than that over pure C12A7−O^- catalyst (e.g., NSC at 550 °C, 95 μmol/g (K_2O) and 22.5 μmol/g (C12A7−O^-)). The NSC of the C12A7−O^-/K catalyst depends on the percentage of potassium, with the optimum doping amount $x = 9.6$ wt % in C12A7−O^-/K. On the basis of the XRD, XPS, and FTIR measurements, NO_3^- formed under oxidizing conditions was the most important NO_x storage intermediate with the C12A7−O^-/K catalyst. It has been well understood that BaO (or $BaCO_3$) acted as the NO_x storage

components on the barium-based catalysts and nitrate/nitrite were formed by the reactions between Ba^{2+} and NO_x.[3−6]

However, it was found that the pure C12A7−O⁻ catalyst possesses a certain activity for NO reduction with good N_2 selectivity. The microporous material $12CaO{\cdot}7Al_2O_3$ (C12A7)[62,63] is characterized by a positively charged lattice framework $[Ca_{24}Al_{28}O_{64}]^{4+}$ including 12 subnanometer-sized cages. The two remaining O^{2-} ions are clathrated in the cages, which are able to substituted by another singly charged anion X^- ($X^- = O^-$, H^-, OH^-, etc.) to form the derivatives $[Ca_{24}Al_{28}O_{64}]^{4+}{\bullet}4(X^-)$ (C12A7−X⁻).[55−56,64] For microporous C12A7−O⁻, the O^- anions can be stored in the cages of C12A7−O⁻ and also be emitted into the gas phase by applying an extraction field at a suitable temperature.[65−67] The active anion species O^- is a key intermediate in the anion chemistry,[40−45] and the material C12A7−O⁻ may be used as an active catalyst.[46] We now consider the mechanism of the selective reduction of NO to N_2 over C12A7−O⁻ by H_2. First, the absorbed NO(s) on the C12A7−O⁻ surface would dissociate into N(s) + O(s) and give N_2 by the N(s) + NO(s) → N_2 + O(s) reaction, which has been proposed to explain the reduction of NO by H_2 over the Pt-based catalyst.[68−70] This route seems unlikely to dominate the reduction of NO with C12A7−O⁻, according to the fact that N_2 cannot be detected in the absence of H_2. The second probable explanation for the reduction of NO by H_2 is NO(s) → NH_x(s) → N_2; however, we failed to confirm the presence of the NH_x-(s) species by quadropole mass spectrometry and other characteristic measurements mentioned above (FTIR and XPS, etc.). The third possible route of NO reduction by H_2 over C12A7−O⁻ would be NO(s) → NO_3^-(s)/NO_2^-(s) → N_2. We think that the third route is the most likely candidate since the NO_2^-(s) and NO_3^-(s) species can be formed from NO(s) + O^-(s) and NO(s) + O_2^-(s), as demonstrated by the anionic TOF measurements for the NO/C12A7−O⁻ system (Figure 16). This proposal is also consistent with the observation that the NO_3^- species is formed in the NO_x storage step (the reactions in NO/O_2/C12A7−O⁻/10%K), which can be completely removed by H_2 (see the XPS and FTIR characteristic results). Moreover, the activation of adsorbed NO followed by the reaction with H_2 (i.e., NO(s) + H → N_2) is also possible to contribute to the NO reduction.[70] Thus, the third route (i.e., NO(s) → NO_3^-(s)/NO_2^-(s) → N_2) and the last one are most likely to account for the reduction of NO by H_2 over the C12A7−O⁻ and C12A7−O⁻/K catalysts.

We have shown that K_2O was able to store NO_x as nitrate or nitrite. Although K_2O itself had a much lower activity for NO reduction, it was noted that the addition of potassium significantly promoted both the reduction of NO and the selectivity to N_2 rather than to N_2O for the K-doped C12A7−O⁻ catalyst (i.e., C12A7−O⁻/K). However, the ignition temperature for NO reduction obviously dropped by adding potassium to the pure C12A7−O⁻ catalyst. The optimum percentage of potassium is about $x = 10$ wt % in C12A7−O⁻/K based on the overall evaluation for the NO_x storage capacity, the NO reduction ability, and the N_2 selectivity. The influence of the alkali metals' addition (in particular sodium) on the performance of NO reduction by H_2 has been studied previously.[57,71−72] Marina et al.[71] have reported that the addition of Na promotes the reduction activity of NO and the selectivity to N_2 for a Pt film deposited on Al_2O_3. Burch et al.[57] have found that small amounts of Na enhanced the activity but larger loadings led to poisoning of the Pt/Al_2O_3 catalyst. However, Machida et al.[72] have reported that larger Na loadings (10−15 wt %) on the Pt/Na/ZSM-5 system significantly enhanced the NO reduction and the N_2 selectivity. Our results also suggest that the addition of potassium (5−13 wt %) on the C12A7−O⁻/K catalyst favor the selective reduction of NO to N_2. The reason for the promotion effect of the alkali metals is not well understood at the moment, but probable explanations include modification of the acid−base properties of the material and enhancement of the adsorption and dissociation of NO.[72]

As a summary of the NO_x storage/reduction mechanism, we suggested that NO was first adsorbed on the K_2O and C12A7−O⁻ sites of C12A7−O⁻/K and mainly converted to NO_3^- and/or NO_2^- as NO_x storage intermediates. These species can be reduced by a reducing agent (e.g., hydrogen). The main NO_x storage/reduction routes would be expressed as follows:

(1) NO_x storage mechanism

$$NO(g) \rightarrow NO(s) \tag{3}$$

$$O_2(g) \rightarrow O_2(s) \tag{4}$$

$$NO(s) + O^-(s) \rightarrow NO_2^-(s) \tag{5}$$

$$NO_2^-(s) + {}^1/_2O_2(s) \rightarrow NO_3^-(s) \tag{6}$$

$$NO(s) + O_2^-(s) \rightarrow NO_3^-(s) \tag{7}$$

$$NO(s) + {}^1/_2O_2(s) \rightarrow NO_2(s) \tag{8}$$

$$K_2O(s) + 2NO_3^- \rightarrow 2KNO_3(s) + O^{2-} \tag{9}$$

$$K_2O(s) + NO(s) \rightarrow KNO_2(s) \tag{10}$$

$$K_2O(s) + 2NO_2(s) + {}^1/_2O_2(s) \rightarrow 2KNO_3(s) \tag{11}$$

(2) NO reduction mechanism by H_2

$$H_2(g) \rightarrow H_2(s) \tag{12}$$

$$H_2(s) \rightarrow 2H(s) \tag{13}$$

$$NO_3^-(s) + H_2(s) \rightarrow NO_2^-(s) + H_2O(g) \tag{14}$$

$$2NO_3^-(s) + 5H_2(s) \rightarrow O^{2-}(s) + N_2(g) + 5H_2O(g) \tag{15}$$

$$2NO_3^-(s) + 4H_2(s) \rightarrow O^{2-}(s) + N_2O(g) + 4H_2O(g) \tag{16}$$

$$2NO_2^-(s) + 3H_2(s) \rightarrow O^{2-}(s) + N_2(g) + 3H_2O(g) \tag{17}$$

$$2NO_2^-(s) + 2H_2(s) \rightarrow O^{2-}(s) + N_2O(g) + 2H_2O(g) \tag{18}$$

$$2NO(s) + 4H(s) \rightarrow N_2(g) + 2H_2O(g) \tag{19}$$

$$2NO(s) + 2H(s) \rightarrow N_2O(g) + H_2O(g) \tag{20}$$

where g and s stand for the species in the gas phase and on the catalyst surface, respectively. In addition, these reactions may also occur in the body of the sample. Definitely, further work is needed to clarify the NO_x storage and reduction processes.

However, the sulfur tolerance feature is one of most important factors for a NO_x storage/reduction catalyst. We have found that C12A7−O⁻/K had good resistance to sulfur poisoning under the initial NO_x storage/reduction procedures. However, the sulfur

tolerance mechanism for C12A7−O^-/K is not clear, and it should be further studied.

4. Conclusion

The C12A7−O^-/K catalyst shows good NO_x storage/reduction abilities with a good sulfur tolerance. Over 50% of NO can be reduced to N_2 by H_2 as a reduction agent at 550−700 °C. The NO conversion and N_2 selectivity on the C12A7−O^-/K catalyst mainly depends on the sample temperature, percentage of potassium, the reduction agent, and the composition in the mixture gases. The C12A7−O^-/10%K catalyst shows the highest NO conversion to N_2 among the catalysts C12A7−O^-/*x*%K. The N_2 selectivity increases with increasing temperature below 600 °C, giving a maximum value close to 100% at about 600 °C. An optimum temperature window for NO reduction to N_2 with the C12A7−O^-/10%K catalyst ranges from 500 to 700 °C. However, an optimum temperature window for NO_x storage with the C12A7−O^-/10%K catalyst ranges from 400 to 650 °C. It was identified that the active oxygen species, K_2O, and NO_3^- were very important intermediates on the C12A7−O^-/10%K catalyst for the NO_x storage/reduction process. We suggested that NO was first adsorbed on the K_2O and C12A7−O^- sites, and mainly converted to NO_3^- and/or NO_2^- as NO_x storage intermediates. Most of the NO_x storage intermediates can be reduced to N_2 by the reducing agents (e.g., H_2 and hydrocarbons) under the optimum reduction conditions.

Acknowledgment. We thank Professor Y. L. Fu for helpful discussions. Q. X. Li is thankful for the support of the "BRP Program 2002" and the "Innovation Program 2002" by the Chinese Academy of Sciences.

References and Notes

(1) Toyota Jidosha Kabusjiki. Jpn. Patent No. EP658370, 1994.
(2) Miyoshi, M.; Matsumoto, S.; Katoh, K.; Tanaka, T.; Harada, J.; Takahashi, N.; Yokota, K.; Suguira, M.; Kasahara, K. *Development of New Concept Three-Way Catalyst for Automotive Lean−Burn Engines*; SAE Technical Paper 950809; Society of Automotive Engineers: Warrendale, PA, 1995.
(3) Takahashi, N.; Shinjoh, H.; Iijima, T.; Suzuki, T.; Yamazaki, K.; Yokota, K.; Suzuki, H.; Miyoshi, M.; Matsumoto, M.; Tanizawa, T.; Tanaka, T.; Tateishi, S.; Kasahara, K. *Catal. Today* **1996**, *27*, 63.
(4) Mahzoul, H.; Gilot, P.; Brilhac, J. F.; Stanmore, B. R. *Top. Catal.* **2001**, *16/17*, 293.
(5) Liu, Z. Q.; Anderson, J. A. *J. Catal.* **2004**, *224*, 18.
(6) Nova, I.; Castoldi, L.; Lietti, L.; Tronconi, E.; Forzatti, P. *Catal. Today* **2002**, *75*, 431.
(7) Fridell, E.; Persson, H.; Westerberg, B.; Olsson, L.; Skoglundh, M. *Catal. Lett.* **2000**, *66*, 71.
(8) Carabineiro, S. A.; Fernandes, F. B.; Vital, J. S.; Ramos, A. M.; Silva, I. F. *Catal. Today* **1999**, *54*, 559.
(9) Fridell, E.; Skoglundh, M.; Westerberg, B.; Johansson, S.; Smedler, G. *J. Catal.* **1999**, *183*, 196.
(10) Mahzoul, H.; Brilhac, J. F.; Gilot, P. *Appl. Catal., B* **1999**, *20*, 47.
(11) Amberntsson, A.; Skoglundh, M.; Ljungstrom, S.; Fridell, E. *J. Catal.* **2003**, *217*, 253.
(12) Amberntsson, A.; Fridell, E.; Skoglundh, M. *Appl. Catal., B* **2003**, *46*, 429.
(13) Westerberb, B.; Fridell, E. *J. Mol. Catal. A: Chem.* **2001**, *165*, 249.
(14) Vijay, R.; Hendershot, R. J.; Jimenez, S. M. R.; Rogers, W. B.; Feist, B. J.; Snively, C. M.; Lauterbach, J. *Catal. Commun.* **2005**, *6*, 167.
(15) Clacens, J. M.; Montiel, R.; Kochkar, H.; Figueras, F.; Guyon, M.; Beziat, J. C. *Appl. Catal., B* **2004**, *53*, 21.
(16) Vaezzadeh, K.; Petit, C.; Pitchon, V.; Kiennemann, A. *Catal. Commun.* **2002**, *3*, 179.
(17) Obuchi, A.; Ogata, A.; Mizuno, K.; Ohi, A.; Nakamura, M.; Ohuchi, H. *J. Chem. Soc., Chem. Commun.* **1992**, 247.
(18) Horose, H.; Yahiro, H.; Mizuno, N.; Iwamoto, M. *Chem. Lett.* **1991**, 1859.
(19) Li, Y.; Armor, J. N. *Appl. Catal., B* **1993**, *2*, 239.
(20) Witzel, F.; Sill, G. A.; Hall, W. K. *J. Catal.* **1994**, *149*, 229.
(21) Iwamoto, M.; Yahiro, H. *Catal. Today* **1994**, *22*, 5.
(22) Ohno, T.; Hatayama, F.; Toda, Y.; Konishi, S.; Miyata, H. *Appl. Catal., B* **1995**, *5*, 89.
(23) Bosch, H.; Janssen, F. J. J. G. *Catal. Today* **1988**, *2*, 369.
(24) Amiridis, M. D.; Zhang, T. J.; Farrauto, R. J. *Appl. Catal., B* **1996**, *10*, 203.
(25) Ribotta, A.; Lezcano, M.; Kurgansky, M.; Miro, E.; Lombardo, E.; Petunchi, J.; Moreaux, C.; Dereppe, J. M. *Catal. Lett.* **1997**, *49*, 77.
(26) Ohtsuka, H.; Tabata, T. *Appl. Catal., B* **1999**, *21*, 133.
(27) Sullivan, J. A.; Cunningham, J. *Appl. Catal., B* **1998**, *15*, 275.
(28) Long, R.; Yang, R. T. *Catal. Lett.* **1998**, *52*, 91.
(29) Burch, R.; Watling, T. C. *J. Catal.* **1997**, *169*, 45.
(30) Burch, R.; Sullivan, J. A.; Watling, T. C. *Catal. Today* **1998**, *42*, 13.
(31) Kameoka, S.; Chafik, T.; Ukisu, Y.; Miyadera, T. *Catal. Lett.* **1998**, *55*, 21.
(32) Shimizu, K. I.; Satsuma, A.; Hattori, T. *Appl. Catal., B* **2000**, *25*, 239.
(33) Otto, K.; Yao, H. C. *J. Catal.* **1980**, *66*, 229.
(34) Sharpe, R. G.; Bowker, M. *Surf. Sci.* **1996**, *360*, 21.
(35) Burch, R.; Coleman, M. D. *Appl. Catal., B* **1999**, *23*, 115.
(36) Amberntsson, A.; Skoglundh, M.; Jonsson, M.; Fridell. E. *Catal. Today* **2002**, *73*, 279.
(37) Fridell, E.; Persson, H.; Olsson, L.; Westerberg, B.; Amberntsson, A.; Skoglundh, M. *Top. Catal.* **2001**, *16/17*, 133.
(38) Yamazaki, K.; Suzuki, T.; Takahashi, N. *Appl. Catal., B* **2001**, *30*, 459.
(39) Matsumoto, S.; Ikeda, Y.; Suzuki, H.; Ogai, M.; Miyoshi, N. *Appl. Catal., B* **2000**, *25*, 115.
(40) Fessenden, R. W.; Meisel, D. *J. Am. Chem. Soc.* **2000**, *122*, 3773.
(41) Lee, J.; Grabowski, J. J. *Chem. Rev.* **1992**, *92*, 1611.
(42) Born, M.; Ingemann, S.; Nibbering, N. M. M. *Mass Spectrom. Rev.* **1997**, *16*, 181.
(43) Tashiro, T.; Watanabe, T.; Kawasaki, M.; Toi, K. *J. Chem. Soc., Faraday Trans.* **1993**, *89*, 1263.
(44) Aika, K.; Lunsford, J. H. *J. Phys. Chem.* **1977**, *81*, 1393.
(45) Neophytides, S. G.; Tsiplakides, D.; Stonehart, P.; Jaksic, M. M.; Vayenas, C. G. *Nature* **1994**, *370*, 45.
(46) Dong, T.; Li, J.; Huang, F.; Wang, L.; Tu, J.; Torimoto, Y.; Sadakata, M.; Li, Q. X. *Chem. Commun.* **2005**, *21*, 2724.
(47) Li, X. G.; Meng, M.; Lin, P. Y.; Fu, Y. L.; Hu, T.; Xie, Y. N.; Zhang, J. *Chem. Eng. Res. Des.* **2002**, *80*, 190.
(48) Li, X. G.; Meng, M.; Lin, P. Y.; Fu, Y. L.; Hu, T.; Xie, Y. N.; Zhang, J. *Top. Catal.* **2003**, *22*, 111.
(49) Li, X. G.; Chen, J. F.; Lin, P. Y.; Meng, M.; Fu, Y. L.; Tu, J.; Li, Q. X. *Catal. Commun.* **2004**, *5*, 25.
(50) Gao, A. M.; Lin, P. Y.; Tu, J.; Meng, M.; Li, Q. X. *Chin. J. Chem. Phys.* **2004**, *17*, 485.
(51) Huang, F.; Li, J.; Wang, L.; Dong, T.; Tu, J.; Torimoto, Y.; Sadakata, M.; Li, Q. X. *J. Phys. Chem. B* **2005**, *109*, 12032.
(52) Li, J.; Huang, F.; Wang, L.; Wang, Z. X.; Yu, S. Q.; Torimoto, Y.; Sadakata, M.; Li, Q. X. *J. Phys. Chem. B* **2005**, *109*, 14599.
(53) Li, J.; Huang, F.; Wang, L.; Yu, S. Q.; Torimoto, Y.; Sadakata, M.; Li, Q. X. *Chem. Mater.* **2005**, *17*, 2771.
(54) Huang, F.; Li, J.; Xian, H.; Tu, J.; Sun, J. Q.; Yu, S. Q.; Li, Q. X.; Torimoto, Y.; Sadakata, M. *Appl. Phys. Lett.* **2005**, *86*, 114101.
(55) Li, Q. X.; Hayashi, K.; Nishioka, M.; Kashiwagi, H.; Hirano, M.; Torimoto, Y.; Hosono, H.; Sadakata, M. *Appl. Phys. Lett.* **2002**, *80*, 4259.
(56) Li, Q. X.; Hosono, H.; Hirano, M.; Hayashi, K.; Nishioka, M.; Kashiwagi, H.; Torimoto, Y.; Sadakata, M. *Surf. Sci.* **2003**, *527*, 100.
(57) Burch, R.; Coleman, M. D. *J. Catal.* **2002**, *208*, 435.
(58) Schroeder, R. A.; Lyons, L. L. *J. Inorg. Nucl. Chem.* **1966**, *28*, 1155.
(59) Davydov,A. A. *Infrared Spectroscopy of Adsorbed Species on the Surface of Transition Metal Oxides*; Wiley: New York, 1990.
(60) Kikuyama, S.; Matsukuma, I.; Kikuchi, R.; Sasaki, K.; Eguchi, K. *Appl. Catal., A* **2002**, *226*, 23.
(61) Schmitz, P. J.; Baird, R. J. *J. Phys. Chem. B* **2002**, *106*, 4172.
(62) Hosono, H.; Abe, Y. *Inorg. Chem.* **1987**, *26*, 1192.
(63) Hayashi, K.; Matsuishi, S.; Ueda, N.; Hirano, M.; Hosono, H. *Chem. Mater.* **2003**, *15*, 1851.
(64) Toda, Y.; Matsuishi, S.; Hayashi, K.; Ueda, K.; Kamiya, T.; Hirano, M.; Hosono, H. *Adv. Mater.* **2004**, *16*, 685.
(65) Mukhopadhyay, R.; kunzru, D. *Ind. Eng. Chem. Res.* **1993**, *32*, 1914.
(66) Kumar, V. A.; Pant, K. K.; Kunzru, D. *Appl. Catal., A* **1997**, *162*, 193.
(67) Pant, K. K.; Kunzru, D. *Ind. Eng. Chem. Res.* **1997**, *36*, 2059.
(68) Burch, R.; Shestov, A. A.; Sullivan, J. A. *J. Catal.* **1999**,*186*, 353.
(69) Shestov, A. A.; Burch, R.; Sullivan, J. A. *J. Catal.* **1999**,*186*, 362.
(70) Shibata, J.; Hashimoto, M.; Shimizu, K.; Yoshida, H.; Hattori, T.; Satsuma, A. *J. Phys. Chem. B* **2004**, *108*, 18327.
(71) Marina, O. A.; Yentekakis, I. V.; Vayenas, C. G.; Palermo, A.; Lambert, R. M. *J. Catal.* **1997**, *166*, 218.
(72) Machida, M.; Watanabe, T. *Appl. Catal., B* **2004**, *52*, 281.